The ISME Journal (2013) 7, 1997–2009

www.nature.com/ismej

ORIGINAL ARTICLE

Specific carbonate–microbe interactions in the modern microbialites of Lake Alchichica (Mexico)

Emmanuelle Gérard[1], Bénédicte Ménez[1], Estelle Couradeau[1,2,3], David Moreira[3], Karim Benzerara[2], Rosaluz Tavera[4] and Purificación López-García[3]

[1]*Géobiosphère Actuelle et Primitive, Institut de Physique du Globe de Paris, CNRS UMR 7154, Université Paris Diderot, Sorbonne Paris Cité, Paris, France;* [2]*Laboratoire de Minéralogie et de Physique des Milieux Condensés UMR 7590 CNRS, Université Pierre et Marie Curie, Paris, France;* [3]*Unité Ecologie Systématique et Evolution, CNRS, UMR 8079 Université Paris-Sud, Orsay, France and* [4]*Departamento de Ecología y Recursos Naturales, Universidad Nacional Autónoma de México, Mexico, Mexico*

The role of microorganisms in microbialite formation remains unresolved: do they induce mineral precipitation (microbes first) or do they colonize and/or entrap abiotic mineral precipitates (minerals first)? Does this role vary from one species to another? And what is the impact of mineral precipitation on microbial ecology? To explore potential biogenic carbonate precipitation, we studied cyanobacteria–carbonate assemblages in modern hydromagnesite-dominated microbialites from the alkaline Lake Alchichica (Mexico), by coupling three-dimensional imaging of molecular fluorescence emitted by microorganisms, using confocal laser scanning microscopy, and Raman scattering/spectrometry from the associated minerals at a microscale level. Both hydromagnesite and aragonite precipitate within a complex biofilm composed of photosynthetic and other microorganisms. Morphology and pigment-content analysis of dominant photosynthetic microorganisms revealed up to six different cyanobacterial morphotypes belonging to Oscillatoriales, Chroococcales, Nostocales and Pleurocapsales, as well as several diatoms and other eukaryotic microalgae. Interestingly, one of these morphotypes, *Pleurocapsa*-like, appeared specifically associated with aragonite minerals, the oldest parts of actively growing *Pleurocapsa*-like colonies being always aragonite-encrusted. We hypothesize that actively growing cells of Pleurocapsales modify local environmental conditions favoring aragonite precipitation at the expense of hydromagnesite, which precipitates at seemingly random locations within the biofilm. Therefore, at least part of the mineral precipitation in Alchichica microbialites is most likely biogenic and the type of biominerals formed depends on the nature of the phylogenetic lineage involved. This observation may provide clues to identify lineage-specific biosignatures in fossil stromatolites from modern to Precambrian times.

The ISME Journal (2013) **7,** 1997–2009; doi:10.1038/ismej.2013.81; published online 27 June 2013
Subject Category: Geomicrobiology and microbial contributions to geochemical cycles
Keywords: microbialites; Pleurocapsales; aragonite; hydromagnesite; Raman spectroscopy; confocal laser scanning microscopy

Introduction

Microbialites are organosedimentary structures formed by the direct and/or indirect activity of associated microorganisms. They can be laminated in the case of stromatolites. Although abundant in the Precambrian, microbialites are scarce today, being found only in restricted areas such as in the hypersaline Shark Bay in Australia (Logan, 1961) and in alkaline lakes such as Lake Van in Turkey (Kempe *et al.*, 1991) or Lake Satonda in Indonesia (Arp *et al.*, 2003). The stromatolites from the Bahamas are the only example of such structures developing in an open marine environment (Dravis, 1983; Dill *et al.*, 1986; Reid and Browne, 1991; Reid *et al.*, 2000, 2003). Modern microbialites can be used as analogs of the oldest fossil stromatolites, which can be traced back to the early Archean at 3.5 billion years (Awramik and Sprinkle, 1999). However, the biogenic origin of the oldest fossil stromatolites is still debated, as microfossils or other indisputable biosignatures are not systematically and unambiguously associated with them (for example, Buick *et al.*, 1981; Grotzinger and Knoll, 1999; Lepot *et al.*, 2008, 2009). For this reason, the physical, chemical and biological processes that control the growth of modern stromatolites remain to be properly understood. In particular, the specific role of microorganisms in the formation of stromatolites remains

Correspondence: E Gérard, Géobiosphère Actuelle et Primitive, Institut de Physique du Globe de Paris, CNRS UMR 7154, Université Paris Diderot, Sorbonne Paris Cité, 1, Rue jussieu, 75238 Paris, France.
E-mail: emgerard@ipgp.fr
Received 12 December 2012; revised 22 March 2013; accepted 17 April 2013; published online 27 June 2013

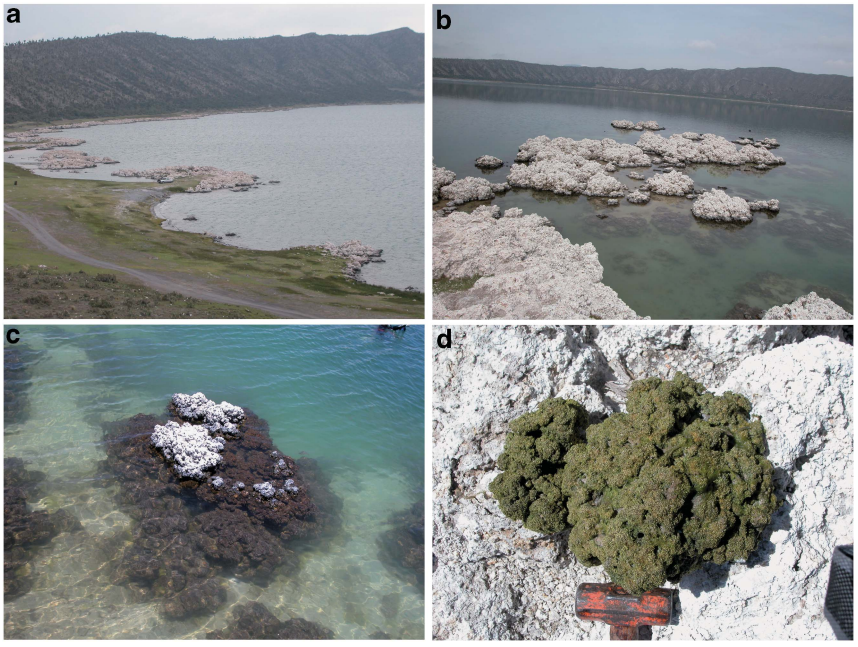

Figure 1 General views of microbialites from the Alchichica Lake. (**a**) Overview of the lake surrounded by white emerged subfossil microbialites mainly composed of hydrated Mg carbonates, namely hydromagnesite. (**b** and **c**) Closer views of white subfossil microbialites from the lake bank and dark microbialites covered by biofilms below the lake surface. (**d**) Green microbialite fragment sampled between 6 and 8 m water depth.

elusive, that is, whether they have a direct role by promoting carbonate precipitation, or an indirect role by secondarily colonizing abiotically precipitated minerals, and eventually stabilizing and further entrapping abiotic precipitates. Some metabolisms, such as photosynthesis and sulfate reduction, are known to promote carbonate precipitation by local alkalinization (that is, pH increase), whereas others, such as aerobic heterotrophy or fermentation, promote carbonate dissolution by acidification (Dupraz and Visscher, 2005; Dupraz *et al.*, 2009). Exopolymeric substances (EPSs), consisting a mixture of carbohydrates, proteins and nucleic acids, excreted in various amounts, are also known to have a negative or positive role in carbonate formation, depending on their divalent cation binding capacity, rendering Ca^{2+} or Mg^{2+}, available or not, for precipitation (Braissant *et al.*, 2007, 2009; Dupraz *et al.*, 2009). In addition, microbial activity may lead to the formation of particular mineralogical structures, which, when associated with remnants of cells or organic polymers, could be used as biosignatures of the past life on Earth and/or, possibly, other planets (for example, Benzerara *et al.*, 2006; Benzerara and Menguy, 2009; Dupraz *et al.*, 2009).

In the aim to detect particular mineral–microorganism associations that might indicate the biogenicity of some mineral phases and point out to a direct role of microorganisms in microbialite formation we have looked for specific mineral–microbe associations in modern microbialites collected from the alkaline (pH 8.9) crater lake of Alchichica located near Puebla, Mexico (Kaźmierczak *et al.*, 2011). This lake is carbonate-enriched and exhibits a Mg/Ca ratio of *ca.* 40. Under these conditions, the precipitation of hydromagnesite ($Mg_5(CO_3)4(OH)2 + 4H_2O$), which is the dominant carbonate mineral in microbialites, is naturally favored (Kaźmierczak *et al.*, 2011). Alchichica microbialites harbor a wide diversity of cyanobacteria, among which members of the Oscillatoriales and Pleurocapsales are the most abundant, but also members of many other prokaryotic and eukaryotic lineages are present (Couradeau *et al.*, 2011, 2012).

To look for specific mineral–microbe interactions in Alchichica microbialites, we used a novel methodological approach for the three-dimensional imaging of microbialites combining confocal laser scanning microscopy (CLSM) observations and Raman spectroscopy at the micrometric scale.

CLSM has been traditionally used to image naturally autofluorescent, pigment-bearing microorganisms, such as cyanobacteria, but also is used to image microorganisms labeled with specific fluorescent probes, for example, during fluorescent *in situ* hybridization experiments (see Kawaguchi and Decho, 2002; Amann and Fuchs, 2008; Goh *et al.*, 2009). The spectrum of the Raman-scattered light is specific of the chemical bonds and symmetry of molecules, allowing the spectra to be used to identify a wide range of abiotic and biotic materials (Beyssac and Lazzeri, 2012). Raman spectroscopy has been increasingly used indeed to correlate macromolecular composition with specific microorganisms in natural communities (Huang *et al.*, 2007, 2009, 2010; Wagner, 2009; Wagner *et al.*, 2009; Hall *et al.*, 2010) and is particularly relevant to

identify and map minerals, including polymorphs of calcium carbonate, such as aragonite and calcite (Rividi *et al*., 2010).

By combining CLSM and Raman spectroscopy, we show that although hydromagnesite is associated with the EPS of various cyanobacteria and other microorganisms, aragonite is closely related to one cyanobacterial morphotype belonging to the order Pleurocapsales. This strongly suggests that these cyanobacteria promote the precipitation of carbonates in Alchichica microbialites, and that the nature of precipitated carbonates is specifically linked to their phylogeny.

Materials and methods

Sample collection and fixation

Microbialites and associated biofilms were collected in June 2007 in the alkaline crater lake of Alchichica located in the Cuenca Oriental region (19° 24' N, 98° 24' W) at an altitude of 2300 m (Figures 1a–d). Sampling was carried out from the lake surface down to a 14-m water depth. The lake had a pH of 8.8 with a Mg/Ca ratio of 48 (Kaźmierczak *et al*., 2011). The bulk mass of the microbialites under the biofilms was white and composed mostly of hydromagnesite. A complete description of the lake chemistry and sampling protocol can be found in Kaźmierczak *et al.* (2011). After collection, some microbialite fragments were directly fixed on the field in RNAlater (Ambion, Inc., Austin, TX, USA). Others were stored in sterile Zip plastic bags and fixed at the Orsay laboratory in a formaldehyde solution at 2% (methanol free, ultra pure; Polysciences, Inc., Warrington, PA, USA) for 4 h at 4 °C, washed in phosphate buffered saline and stored in (1/1) ethanol/phosphate buffered saline at −20 °C until use. Finally, a fragment of a 15-m-deep microbialite collected in 2012 was transferred to a laboratory aquarium and maintained in culture (pH *ca.* 9) as described previously (Couradeau *et al*., 2011).

Calcein staining of microbialite biofilms

Calcein (2,4-bis-[N,N′-di(carbomethyl)-aminomethyl]-flluorescein) binds to Ca^{2+} and Mg^{2+}, and emits fluorescence in the presence of both cations at high pH. Fluorescent calcein incorporates into growing calcium carbonate structures and has been traditionally used for identification and measurement of growth of many animals, including fishes, mammals, gastropods, echinoderms (see Moran, 2000), as well as the detection of growing carbonates around bacteria (Zippel and Neu, 2011). Microbialite fragments (14–15 m depth) fixed in RNAlater or freshly collected from the laboratory aquarium were stained with calcein (0.1 mg ml^{-1}) for 36 h at 4 °C in RNAlater or at room temperature in aquarium water. Microbialite-associated biofilms were then mounted between a glass microscope slide and a glass cover slip for CLSM observations.

Staining and LR-white embedding of fixed microbialites

Before embedding, millimeter-sized pieces of formaldehyde-fixed microbialites were stained with DAPI (4′,6-diamidino-2-phenylindole) at 1 μg ml^{-1} for 2 h at room temperature, and with calcein at 0.1 mg ml^{-1} at 4 °C for 48 h. After staining, microbialite fragments were dehydrated in a gradual series of ethanol baths (30%, 50%, 70%, 90% and 100%), and progressively impregnated with hard grade LR-white resin (Polysciences, Inc.). Briefly, the samples were incubated for 18 h at 4 °C in 1/1 and then in 2/1 mixture of LR-white/ethanol, and finally in pure LR-white resin. After 3 h at room temperature, samples were embedded in pure LR-white resin for 1 h at 40 °C and then for 24 h at 60 °C. After polymerization, transverse sections were cut with a diamond wire and polished (diamond powder 0.25 μm) to a final thickness of about 50 μm. LR-white resin is appropriate for water immersion and offers, in addition, excellent resistance to long-lasting laser exposure, inherent to mapping. Raman analyses are moreover not hampered by excessive fluorescence emission and band interferences, as occurs with many other resins.

Combined CSLM and Raman microspectroscopy and imaging

Biofilms and fixed (RNAlater and formaldehyde) microbialites sampled in the lake at 10 cm to 14 m depth were examined at the Institut de Physique du Globe de Paris, using a FluoView FV1000 CLSM with a spectral resolution of 2 nm and a spatial resolution of 0.2 μm (Olympus, Tokyo, Japan) combined with an Invia Raman Spectrometer (Renishaw, Wotton-under-Edge, UK). The FluoView FV1000 was equipped with a 405-nm laser diode and multiline argon (458, 488 and 515 nm), helium–neon–green (543 nm) and helium–neon–red (633 nm) lasers. Fluorescence image stacks of the microbialite transversal sections or the unstained fresh biofilm were obtained with concomitant excitation at wavelengths of 405, 488 and 543 nm by collecting the emitted fluorescence between 425–475, 500–530 and 560–660 nm, respectively. The fluorescence spectra were recorded between 405 and 800 nm for a specific wavelength excitation with band width analyses of 10 nm and steps of 5 nm. For concomitant CSLM/Raman image acquisitions, a water immersion LUMPLFL 60XW objective (Olympus; ×60 magnification) with numerical aperture of 0.9 was used. For RNAlater-fixed biofilm examination, an oil immersion objective UPLSAPO 60XO (Olympus; ×60 magnification, numerical aperture = 1.35) was used. Three-dimensional images were acquired, visualized and processed using the F10-ASW FLUOVIEW software (Olympus). The Renishaw Invia Raman spectrometer was equipped with a 514-nm Ar laser source and a 785-nm laser diode source. As cyanobacterial

autofluorescence blurs Raman analyses when using the 514 nm laser source, we used the 785 nm laser source instead. Beam centering and Raman spectra calibration were performed daily on a Si-Al microprocessor chip displaying a characteristic Si Raman shift at 520.4 cm^{-1}. Extended mode analysis in the range of 100–3000 cm^{-1} was used to acquire reference spectra. Ten individual accumulations of 10 s integration time were performed in order to obtain each reference spectrum; background was not corrected. Dynamic line-scanning Raman mapping (Renishaw Streamline) was performed in the range 387–1538 cm^{-1} by scanning the sample over selected areas (8 s pt^{-1}) by using a motorized PRIORTM stage allowing XYZ displacements with a submicrometric step precision. Laser intensity was set at 300 mW. Under these conditions, a pinhole allowed for a spatial resolution of 2–3 μm. Light was dispersed by a holographic grating with 1200 grooves per millimeter and the signal was analyzed with a RENCAM charge-coupled device detector. Compositional maps representing the intensity distributions of characteristic peaks were determined using the software Wire 3.2 (Renishaw) based on component analysis, comparing reference spectra with each spectrum composing the hyperspectral map. Spectra collected on Alchichica microbialites were identified by comparison with pure aragonite and hydromagnesite mineral standards from the mineral collections of the University Pierre et Marie Curie (Paris, France) and the French National Museum of Natural History, respectively, and with the RRUFF database (http://rruff.info/; Downs, 2006). Cyanobacteria were not analyzed by Raman spectrometry as done by Huang *et al.* (2007), because the Raman spectra of microbial cells are not distinguishable from the Raman spectra of the LR-white resin. The cell localization relies on their fluorescence emission (cyanobacterial autofluorescence and DAPI staining) and is thus based on CLSM imaging.

Results

We applied Raman spectroscopy and CLSM on exactly the same sample zones at the micrometer scale in order to identify potential specific associations between different microorganisms and carbonate precipitates in Alchichica microbialites. We used a variety of microbialite fragments fixed in formaldehyde, stained with DAPI and calcein and LR-white-embedded, which were representative of the average mineralogical content of all the samples (Kaźmierczak *et al.*, 2011; Couradeau *et al.*, 2013).

Identification of cyanobacteria based on their morphology and pigment content

Cyanobacteria are the dominant photosynthesizers in Alchichica microbialites (Couradeau *et al.*, 2011, Kaźmierczak *et al.*, 2011) and the morphology of some characteristic types is informative for taxonomic classification. We thus used CLSM to assess the taxonomic ascription of individual cyanobacterial cells in thin slides of microbialites that were transversally cut based on morphology, fluorescence properties and comparison with publicly available databases (for example, Algal-ED http://silicasecchidisk.conncoll.edu/Algal-ED_finished.html; Komárek and Hauer, 2011). Although photosynthetic pigments, especially chlorophyll, but also phycobiliproteins, were partly extracted or degraded during embedding in LR-white resin, LR-white-included cyanobacterial cells were still clearly detectable by CSLM because of the fluorescence associated to their sheaths and remaining photosynthetic pigments (Figure 2). In addition, cell morphology was particularly well preserved in formaldehyde-fixed samples embedded in LR-white. This allowed a reliable classification of the morphotypes.

We catalogued up to six different cyanobacterial morphotypes that were labeled Un1 and Un2 for unicellular cyanobacteria, F1 for filamentous cyanobacteria, P1 for Pleurocapsales, and N1 and N2 for Nostocales. The different morphotypes of cyanobacteria and tentative taxonomic identification, as well as their respective occurrences in microbialites from different water depths in the lake are summarized in Table 1. The possible affiliations of the six different morphotypes are compatible with molecular diversity analyses based on 16S ribosomal RNA gene sequencing of lake samples (Couradeau *et al.*, 2011; Kaźmierczak *et al.*, 2011). Some cyanobacterial orders like Pleurocapsales or even genera like *Rivularia/Calothrix* and *Nodularia* were easily recognizable. However, morphology and pigment content are not precise-enough criteria to affiliate unambiguously the morphological types to previously identified specific operational taxonomic units (defined as >97% 16S rRNA gene nucleotide identity).

Pleurocapsa-like cells (P1) were among the most widespread morphotypes, becoming noticeably dominant at 14 m depth. They were easily identifiable by their morphology, as they formed colonies of pseudofilaments and were divided by multiple fission and subsequent liberation of smaller daughter cells (baeocytes; Waterbury and Stanier, 1978), as can be seen in Figures 2a and b. Furthermore, the affiliation of the P1 morphotype to the order Pleurocapsales is supported by a previous analysis of 16S rRNA genes, which showed that Pleurocapsales encompassed the dominant cyanobacterial phylotypes in microbialites sampled at 14 m water depth (Couradeau *et al.*, 2011). Up to five different operational taxonomic units affiliated to the Pleurocapsales in previous studies of the same samples (Couradeau *et al.*, 2011, Kaźmierczak *et al.*, 2011). However, morphology alone is not sufficient to establish a clear correspondence between our P1

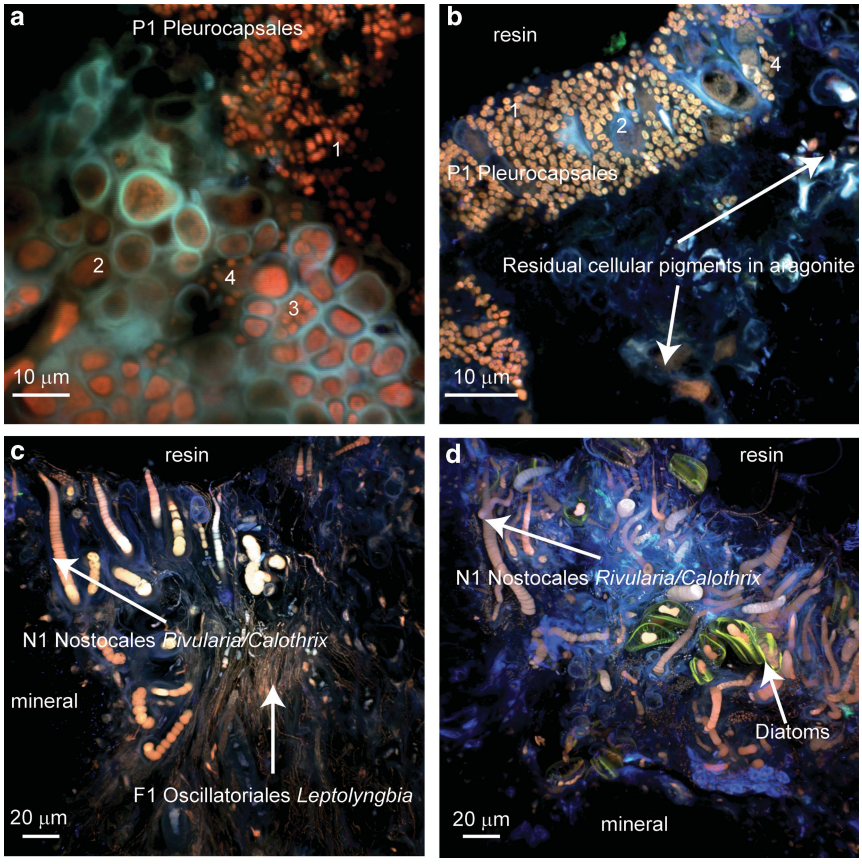

Figure 2 CLSM images showing the major morphotypes of cyanobacteria associated with Alchichica microbialites. Stacked images were obtained with simultaneous excitation at 405, 488 and 543 nm on thin slides of calcein- and DAPI-stained microbialites that were LR-white-embedded and transversally cut. (**a**) Colony of Pleurocapsales likely affiliated to the genus *Pleurocapsa* (14 m water depth). Cells forming pseudofilaments are visible at different developmental stages: (1) baeocytes without any visible sheath, (2) vegetative cell surrounded by sheath, (3) parental cell that has completed division by multiple fissions and is full of baeocytes, (4) disrupted parental cell and free baeocytes. (**b**) Another view of Pleurocapsales cells likely affiliated to the genus *Pleurocapsa* (3–4 m water depth); the numbers refer at the same cellular states as in **a**. (**c** and **d**) Mixed cyanobacterial and probably heterotrophic bacterial biofilm. Filamentous cyanobacteria (F1) may be affiliated to the genus *Leptolyngbia*. These cells produce persistant sheaths. Polar filamentous cyanobacteria (N1) may be affiliated to the genera *Rivularia* or *Calothrix*. These cells produce thicker sheaths and differentiate one heterocyst, where N_2 fixation occurs, devoid of photosynthetic pigments at the larger extremity of the filament. Heterotrophic bacteria appear in blue according to the fluorescence of DAPI. EPS are detectable in blue according to their own fluorescence and DAPI staining. Photosynthetic pigments (chlorophyll a and phycobiliproteins) appear in red and the diatom frustules appear in green.

Table 1 Cyanobacterial morphotypes detected in phototrophic biofilms of Alchichica microbialites based on their morphology and autofluorescence of their pigments

Morphotype name	*Morphology*	*Size*	*Probable identification*	*Localization*
Un1	Unicellular	$L = 2$–5 μm		Al66 (3 m)
Un2	Unicellular with sheath	$Ø = 3$ μm, up to 30 μm	Chroococcales *Gloeocapsa*	Al66 (3 m)
F1	Filamentous with sheath	$Ø = 1$ μm	Oscillatoriales *Leptolyngbya*	Al13 (10 cm), Al 66 (3 m), Al63 (5 m)
P1	Pseudofilamentous with sheath	$Ø = 1$ to 8 μm	Pleurocapsales *Pleurocapsa*	Al13 (10 cm), Al66 (3 m), Al63 (5 m), Al57 (8 m), Al51 (14 m)
N1	Filamentous with polar heterocysts and sheath	$L = 15$ μm	Nostocales *Rivularia*	Al13 (10 cm), Al66 (3 m), Al63 (5 m)
N2	Filamentous with heterocysts and akinetes	$L = 15$ μm	Nostocales *Nodularia*	Al 66 (3 m)

Abbreviations: *Ø*, diameter; *L*, length.
Al followed by a number refers to fixed microbialites from the lake.

morphotype and a particular operational taxonomic unit. It is noteworthy that some Alchichica cyanobacteria, such as *Gloeocapsa*- and *Leptolyngbya*-like species, *Rivularia* and Pleurocapsales, were visibly surrounded by an important amount of EPS, which results in the entrapment of mineral phases (Figure 2 and Supplementary Figure S1).

Fluorescence/Raman imaging of Alchichica microbialites

Combined CLSM and Raman imaging were used to characterize the nature of carbonates forming within the biofilms. Figure 3 displays characteristic Raman spectra associated with the major minerals composing Alchichica microbialites. Hydromagnesite, a hydrated magnesium carbonate ($Mg_5(CO_3)_4(OH)_2{\bullet}4(H_2O)$), was the most abundant one in agreement with previous bulk X-ray diffraction analyses (Kaźmierczak *et al.*, 2011). Aragonite ($CaCO_3$) was also detected, although in less abundance. As shown in Figure 4a, the outer biofilm, mainly formed by Pleurocapsales, was clearly visible on top of the section because of the fluorescence of remnant sheaths and photosynthetic pigments, with a maximum fluorescence emission, remaining after formaldehyde fixation and LR-white embedding, between 450 and 550 nm following an excitation at 405 nm (encircled area 2 in Figures 4a and d and spectrum 2 in Figure 4c). Relics of cellular pigments were also detectable within the mineral matrix (area 3 in Figures 4a and d and spectrum 3 in Figure 4c), showing that cyanobacterial cells were encrusted in the mineralized area. CLSM revealed at least two different types of minerals below the outer overlying biofilm (MM1 and MM2). Superimposition of the CLSM image and the associated Raman map (Figure 4b) showed that the minerals MM1 and MM2 were aragonite and hydromagnesite, respectively. Although hydromagnesite composed most of the microbialite mass, both in the surface (Supplementary Figure S1) and in the internal mineralized parts, aragonite was systematically found in association with P1 Pleurocapsales colonies. In some areas of microbialites developing near the lake surface (10 cm depth), relics of cellular pigments formed lamination patterns within aragonite. This was not observed for hydromagnesite (Figure 4a).

At a closer scale, light-green calcein staining was detected around remnants of cell sheaths in certain zones of dense actively dividing colonies of Pleurocapsales (Figures 5a and b). The calcein staining appeared as a sort of pavement within the mineral matrix (in black in Figures 5a and b). Superimposed Raman maps (Figures 5c–e) showed that the bulk

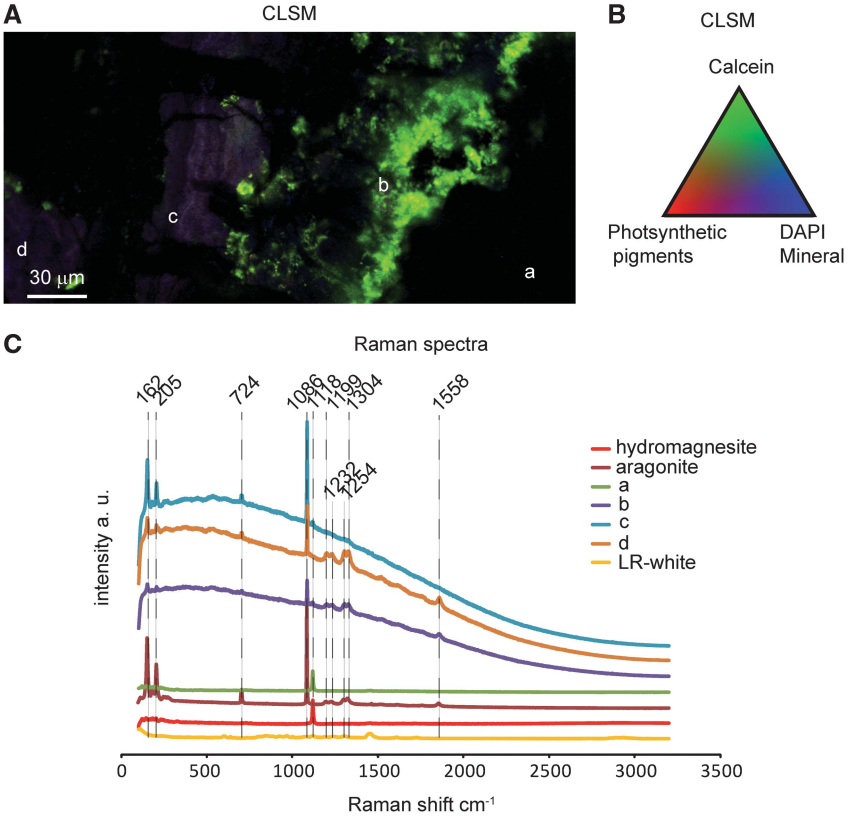

Figure 3 (**A**) CLSM image of LR-white-embedded, calcein- and DAPI-stained microbialite from 10 cm water depth in the lake. The image was obtained by a concomitant excitation at 405, 488 and 543 nm. (**B**) Pseudocolors associated with the components of the image determined by their fluorescence spectra. (**C**) Raw Raman spectra associated with the different areas shown in **A** and references spectra for aragonite, hydromagnesite and LR-white. Background in b, c and d is inherent to the strong fluorescence emitted by the sample.

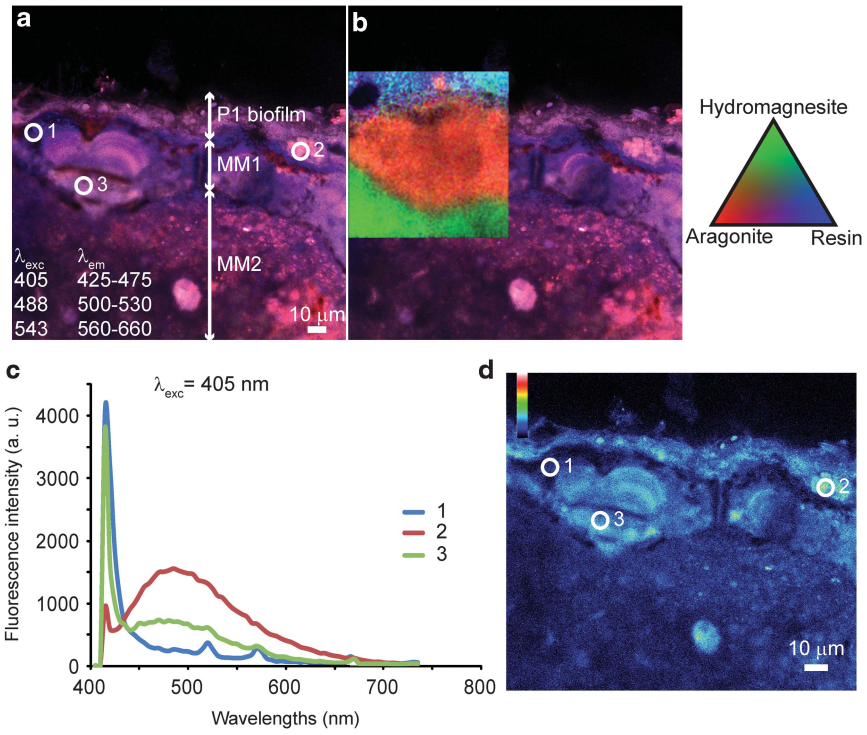

Figure 4 Molecular fluorescence emitted from a transversal section of LR-white–embedded, unstained Alchichica microbialite collected at 10 cm water depth in the lake. (**a**) Image stack obtained with a concomitant excitation at 405, 488, and 543 nm. A biofilm formed mainly of Pleurocapsales is visible in red in the upper part of the section as revealed by the presence of residual photosynthetic pigments. At least two types of minerals can be individualized below the biofilm, noted MM1 and MM2 for mineral matrix areas 1 and 2, respectively. Blue and red fluorescent areas are also detectable within the mineralized part. (**b**) Superimposed tricolor Raman map showing that the mineral matrix is composed of aragonite (MM1, red) and hydromagnesite (MM2, green). Signal emerging from the embedding LR-white resin is shown in blue. (**c**) Fluorescence emission spectra obtained with an excitation at 405 nm collected in the mineral matrix (indexed white circle 1 on panel **a**), the biofilm (circle 2) and the encrusted cells (circle 3), showing that the red fluorescence detected in **a** corresponds to residual photosynthetic pigments. (**d**) Fluorescence maps emitted in the ranges 500–510 nm following an excitation at 405 nm that correspond to the maximum emission for residual photosynthetic pigments and mimic their distributions. In **d**, fluorescence intensities are depicted on a blue–red pseudocolor scale; a. u., arbitrary unit.

part of this mineral matrix was composed of aragonite. We observed the same specific association between Pleurocapsales and aragonite in all the 14 observed sections of field samples collected from 10 cm to 14 m depth (Table 2). These observations combining CLSM and Raman analyses were performed systematically for all the samples over all the areas where the biofilm was detectable, which represented several tens of cubic micrometers for each section. In most of the samples (10 over 14), Pleurocapsales were found in close association with aragonite only, whereas in 4 samples small amounts of hydromagnesite in addition to aragonite were also detected in close association with the Pleurocapsales (for example, Figure 5 and Supplementary Figure S2). We did not observe such aragonite co-occurrence with any other morphotype of cyanobacteria. It is noteworthy that in some microbialite samples, especially those from 14 m depth, the aragonite distribution followed exactly the same pattern as the Pleurocapsales colonies (Figure 6).

A small fraction of hydromagnesite dispersed within aragonite was also detectable in some samples (for example, Figure 5). Notably, hydromagnesite distribution inferred by Raman followed a pavement-like pattern similar to, but not matching exactly with, that shown by calcein staining. More generally, calcein appeared to have a particular affinity for interfaces between aragonite and hydromagnesite (Supplementary Figure S4), and to a lesser extent for hydromagnesite itself (Figure 6 and Supplementary Figure S1).

Rivularia-like cells have been observed previously in aragonite in Alchichica microbialites (Kaźmierczak *et al.*, 2011). In 3 samples out of 14, we similarly detected *Rivularia*-like cells associated with a Pleurocapsales biofilm lying above an aragonite patch. However, in contrast to Pleurocapsales we did not detect *Rivularia* morphotypes alone (that is, without Pleurocapsales) in close association with aragonite.

Calcein staining of microbialite biofilms

In 14- to 15-m-deep microbialite fragments fixed in RNAlater or freshly collected from aquaria enriched in Pleurocapsales colonies, calcein accumulated in the sheaths surrounding the cells, including dividing cells (Figure 7). Baeocytes devoid of

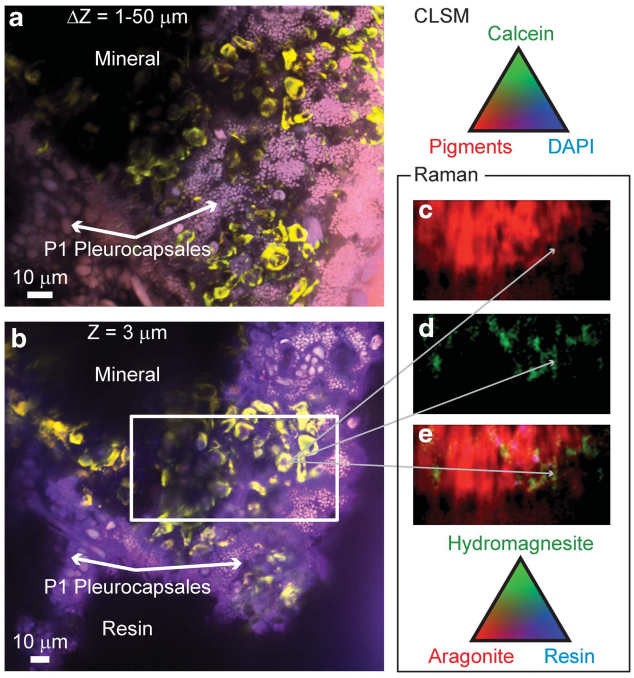

Figure 5 (**a**) Maximum intensity projection of CSLM image stacks obtained on a transversal section of a LR-white-embedded microbialite fragment collected at 10 cm water depth in the lake. It shows an actively growing colony of Pleurocapsales (P1 cells). The sample was stained with DAPI (blue) and calcein (green) before embedding. The CSLM image was obtained over an integrated depth of 50 μm by a concomitant excitation at 405, 488 and 543 nm. Photosynthetic pigments are shown in red. (**b**) Optical section of the Pleurocapsales biofilm at a depth of 3 μm below the surface of the thin section. The white rectangle outlines the area characterized by Raman. Raman-derived aragonite and hydromagnesite maps are displayed in **c** and **d**, respectively. (**e**) Composite tricolor Raman map for aragonite, hydromagnesite and LR-white resin showing the bulk part of the mineral matrix to be composed of aragonite. Hydromagnesite appears scarcer with a distribution pattern close to the CLSM calcein signal. The white dotted arrows indicate corresponding areas in the CSLM and Raman images.

Table 2 Samples analyzed by concomitant Raman CSLM

Sample number	*Depth*	*Association P1–aragonite*	*Association P1–hydromagnesite*
Al13-I1-a	10 cm	+	–
Al13-I1-b	10 cm	+	–
Al13-I2-a	10 cm	+	–
Al13-I2-b	10 cm	+	–
Al13-I2-c	10 cm	+	+
Al13-I3-a	10 cm	+	–
Al69-I1-a	2–3 m	+	+
Al69-I1-b	2–3 m	+	+
Al66-I1-a	3–4 m	+	–
Al63-I1-a	5 m	+	–
Al63-I2-a	5 m	+	–
Al57-I1-a	8 m	+	+
Al51-I1-a	14 m	+	–
Al51-I2-a	14 m	+	–

Abbreviations: CLSM, confocal laser scanning microscopy; P1, Pleurocapsales cells.
Their original depth in the water lake and the type of mineral associated with P1 are indicted (+ for when the cells were found associated with the mineral, – when no association was found).

fluorescently detectable sheaths were not stained by calcein (Figure 7). As only Ca^{2+} and not Mg^{2+} was detectable by scanning electron microscopy and energy-dispersive X-ray spectroscopy around the cells stained with calcein, we concluded that this calcein coloration corresponds to a Ca^{2+} accumulation (Supplementary Figure S2).

Discussion

Despite considerable progress in our understanding of the microbial diversity associated with different microbialites and their mineralogy, the question of whether or not some microorganisms have an important active role in promoting mineral precipitation is unsettled (for example, Reid *et al.*, 2000; López-García *et al.*, 2005). Our study of Alchichica microbialites allows answering partially to this question. Concomitant CSLM and Raman spectroscopy analyses of these microbialites show that both aragonite and hydromagnesite precipitate within the biofilm covering the microbialites. One striking observation is that aragonite appears recurrently associated with one predominant type of cyanobacteria having the typical morphology of Pleurocapsales (Figures 4–6 and Supplementary Figures S3, S4 and S5). So far, few studies have suggested that some species could be specifically associated with mineral precipitation within the complex diversity of a biofilm (for example, Planavsky *et al.*, 2009, Couradeau *et al.*, 2012). Here we show that a specific lineage of cyanobacteria can orient carbonate precipitation towards aragonite, whereas hydromagnesite precipitates elsewhere. Several hypotheses may be considered for the *in situ* precipitation of carbonates within the Alchichica microbialites. The lake is supersaturated with respect to both hydromagnesite and aragonite, but also to other carbonate minerals, such as calcite, as previously described by Kaźmierczak *et al.* (2011). The saturation indexes (SIs), which correspond to log (IAP/K_{sp}), where IAP is the ionic activity product and K_{sp} is the solubility product for each type of mineral, were above zero for both hydromagnesite (SI = 0.68) and aragonite (SI = 0.9). However, precipitation may not occur even if supersaturation is reached because of kinetic barriers, and higher levels of saturation might be needed to overcome kinetic inhibitors. It has been shown, for example, that the SI must exceed 0.8 or 1 for aragonite precipitation to take place (Kempe and Kaźmierczak, 1994; Arp *et al.*, 2001). Biofilm microbiota may overcome these kinetic barriers by changing the chemical balances and supplying nucleation centers for mineral precipitation (for example, Dupraz and Visscher, 2005; Dupraz *et al.*, 2009).

Hydromagnesite is the major carbonate composing Alchichica microbialites, and was observed in the biofilms as few micrometer-sized grains entrapped in EPS produced by cyanobacteria of the

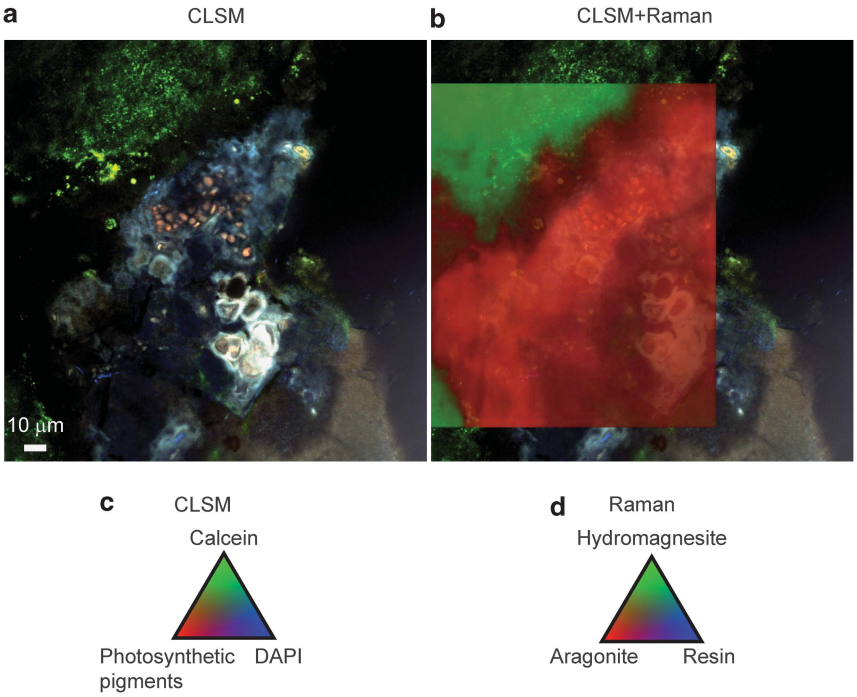

Figure 6 (**a**) CLSM image of LR-white-embedded, calcein- and DAPI-stained microbialite from 14 m water depth obtained by a concomitant excitation at 405, 488 and 543 nm. (**b**) Superimposed composite tricolor Raman map displaying the spatial distribution of aragonite, hydromagnesite and LR-white resin, and showing that the aragonite distribution correlates with the patterns of the Pleurocapsales colony. (**c**) Pseudocolors associated to the components of the CLSM image and identified by their fluorescence spectra. (**d**) Pseudocolors associated to the components of the Raman map as determined by their characteristic Raman spectra.

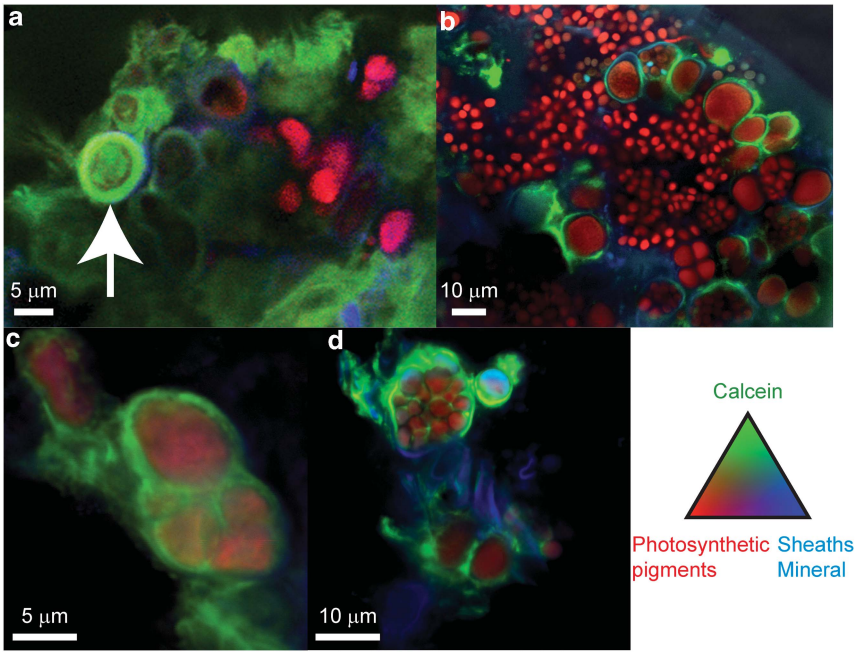

Figure 7 Maximum intensity projection of stacked CLSM images obtained on RNAlater-fixed sample (**a** and **c**) or fresh sample (**b** and **d**) of microbialites from 14 m depth stained with calcein (not embedded). Images were obtained with a sequential excitation at 405, 488 and 543 nm, and fluorescence emission collected in the ranges 425–475, 500–530 and 560–660 nm. The white arrow indicates a cell strongly labeled by calcein.

Leptolyngbya, *Rivularia* genera or Pleurocapsales (Supplementary Figures S1 and S3), or in smaller amounts around Pleurocapsales sheaths (Figure 5). EPS would thus have served as precipitation nuclei, such as that for calcium carbonate precipitation around cyanobacteria (Arp *et al.*, 1999; Braissant *et al.*, 2003; Obst *et al.*, 2009). However, the presence of hydromagnesite does not appear to correlate with

any particular bacterial morphotype and thus seems to be unspecific. EPSs are mainly composed of carbohydrates with small amounts of nucleic acids and proteins, and may contain functional groups such as phosphates and sulfates, which may bind divalent cations. These may be locally concentrated and then released during the degradation of decaying cyanobacterial colonies by heterotrophic bacteria and/or physicochemical degradation (for example, by UV irradiation or changes in pH values), resulting in increased local supersaturation and carbonate precipitation (Decho *et al.*, 2005; Dupraz and Visscher, 2005; Braissant *et al.*, 2007, 2009; Dupraz *et al.*, 2009). This process may be operating in Alchichica microbialites as well. Microorganisms without detectable photosynthetic pigments, probably heterotrophic, were abundantly detected by DAPI coloration in the biofilms (Supplementary Figure S5) and also by bulk molecular diversity methods (Couradeau *et al.*, 2011). Three processes may thus participate in hydromagnesite precipitation in the biofilm: (i) EPS may serve as a matrix and microbial cells as nucleation center for its precipitation, (ii) degradation of EPSs, such as (at least) those of *Leptolyngbya* persistent sheaths may create localized areas where the SI for hydromagnesite precipitation is reached when Mg^{2+} is released and (iii) hydromagnesite precipitates abiotically in the lake and microbial cells grow onto it, but also some, such as those of *Leptolyngbia* and Pleurocapsales, may have a cohesive role by entrapping hydromagnesite grains within the biofilm.

Kaźmierczak *et al.* (2011) proposed that hydromagnesite replaced aragonite rapidly through a syngenetic–diagenetic process occurring in Alchichica microbialites. This would likely explain why aragonite is mostly found at the surface of the microbialites just below the Pleurocapsales biofilm. However, this diagenetic origin could only explain part of the hydromagnesite observed in Alchichica microbialites. Indeed, some hydromagnesite was observed within many biofilms in close association with several morphotypes of cells, suggesting that hydromagnesite might also form authigenetically within living biofilms.

Unlike hydromagnesite, aragonite was observed to be specifically and systematically associated with actively dividing Pleurocapsales. Different textures of aragonite were observed. Very often, fossilized Pleurocapsales cells were clearly visible in the aragonite matrix (for example, Figures 6 and 8; Couradeau *et al.*, 2013), whereas in other cases we only detected residual photosynthetic pigments forming laminations in aragonite (Figure 4 and Supplementary Figure S4). These different patterns could be due to different rates of aragonite precipitation or different states of aragonite diagenesis (Kah and Knoll, 1996; Knoll and Semikhatov, 1998). Considering the taxonomic specificity linked to aragonite precipitation, a biogenic origin for this mineral in Alchichica microbialites is the most likely hypothesis. Different mechanisms can be hypothesized to explain this specificity. It is already known that photosynthesis may promote the precipitation of Ca^{2+} carbonates by increasing the alkalinity through the consumption of CO_2 from HCO_3^- liberating OH^- (Dupraz and Visscher, 2005; Ludwig *et al.*, 2005; Kremer *et al.*, 2008). However, if photosynthesis was the only factor needed to promote aragonite precipitation, this mineral should be observed in association not only with the Pleurocapsales but also with the rest of cyanobacteria. Other processes need, thus, to be considered to explain the specific association of Pleurocapsales with aragonite.

An alternative or additional explanation concerns Ca^{2+}, which accumulates around certain Pleurocapsales cells (Figure 7). It may be argued that actively dividing Pleurocapsales cells preferentially accumulate Ca^{2+} rather than Mg^{2+} in their sheaths. Pleurocapsales harbor indeed a particular cell wall structure with a third external fibrous layer (F-layer) not present in the other cyanobacterial phyla (Waterbury and Stanier, 1978; Büdel and Rhiel, 1985). We showed that newly liberated baeocytes are not stained by calcein. Interestingly, those baeocytes are devoid of the F-layer and Ca^{2+} may accumulate preferentially in this Pleurocapsales-specific structure. The F-layer develops on growing baeocytes that lose their mobility and is thicker around older cells, maintaining them stuck together and to their substrate (Waterbury and Stanier, 1978). This particular F-layer was shown to be formed by a complex organization of globular particles associated in parallel rows in the genus *Chrooccidiopsis* (Büdel and Rhiel, 1985). Furthermore, we showed that aragonite precipitates first as needles around the Pleurocapsales cells from Alchichica microbialites (Couradeau *et al.*, 2013), which, again, suggest that nucleation occurs in the F-layer joining the cells together. Therefore, the composition of this F-layer seems to specifically favor the precipitation of calcium carbonate instead of magnesium carbonate around Pleurocapsales. Aragonite precipitation is favored over calcite because the still relatively high Mg^{2+} concentration existing in the F-layer in the Alchichica Lake may inhibit calcite precipitation (Deleuze and Brantley, 1997; Stanley and Hardie, 1999). Similarly, it has been already shown that the surface layer of *Synechococcus* strain GL24, made up of identical proteins joined together to form a symmetrical pattern, exhibits selectivity with respect to the ions bound, and preferentially binds Ca^{2+} rather than Mg^{2+} (Schultze-Lam and Beveridge, 1994). We assume that aragonite starts to precipitate on the F-layer of living, photosynthetically active cells, as very well-preserved pigmented cells are still observed in aragonite (Figure 8; Couradeau *et al.*, 2013). In later stages along a fossilization gradient, cells become fully encrusted and a second type of aragonite crystals (large prismatic crystals instead of thin rods radiating

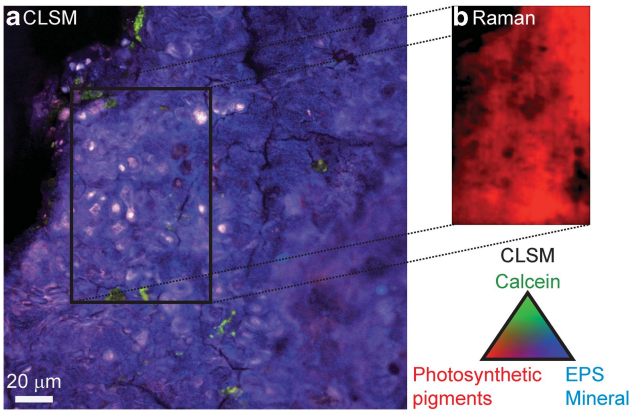

Figure 8 (**a**) CLSM image of LR-white-embedded, calcein- and DAPI-stained microbialite from 10 cm water depth obtained by a concomitant excitation at 405, 488 and 543 nm, showing fossilized Pleurocapsales cells. (**b**) Superimposed composite tricolor Raman map displaying the spatial distribution of aragonite (red), hydromagnesite (green) and LR-white resin (blue).

from the cell wall) occupies the old cytoplasmic space (Couradeau *et al*., 2013).

In summary, Pleurocapsales seem to drive the specific precipitation of aragonite in the presence of natural, high Mg^{2+} concentrations via the concomitant photosynthesis-derived alkalinization of their local environment and the specific accumulation of Ca^{2+} in the F-layer of vegetative cells. In doing so, they become encrusted and progressively fossilize (Couradeau *et al*., 2013). At the same time, increasing carbonate precipitation prevents access to light. Progressive encrustation and increasingly limited access to light may be seen as important selective forces for the evolution of baeocytes. Motile baeocytes, lacking an F-layer, may migrate towards softer, non-encrusted parts of the biofilm where light intensity is more favorable for photosynthesis, thus escaping from complete encrustation in aragonite and allowing the continuous development of the colony. Indeed, we observed that baeocytes were mostly located towards the external part of the biofilm, whereas encrusted cells were towards the interior (Figures 2a and b, and Figure 5).

For a long time, one of the most important questions in stromatolite formation has been (and still is) whether (i) microorganisms develop first and induce carbonate precipitation (directly or indirectly) or whether (ii) carbonate precipitation occurs abiotically and microbes colonize and/or entrap and consolidate the precipitates. Although the two things likely happen *in vivo*, the Pleurocapsales example is a clear case of carbonates formed by microorganisms.

Members of the Pleurocapsales not only seem to be specific active factors in mineral formation in the Alchichica microbialites, as shown by coupled CSLM and Raman spectroscopy, but are also quantitatively abundant in Alchichica and widespread in other microbialite systems. Thus, Pleurocapsales were detected in all microbialite fragments collected in the Alchichica Lake, being dominant at greater depths (Couradeau *et al*., 2011). Furthermore, phylotypes of Pleurocapsales related to those identified in Alchichica microbialites have been detected in numerous other microbialite systems, such as in Lake Van, Turkey (López-García *et al*., 2005), Lake Satonda, Indonesia (Kempe and Kaźmierczak, 1993), Shark Bay, Australia (Goh *et al*., 2009) and the Bahamian stromatolites (Foster *et al*., 2009). Therefore, Pleurocapsales, being abundant, closely associated with the mineral phase and actively promoting mineral precipitation, seem particularly well adapted to microbialite ecosystems and have an important role as ecological architects of microbialite structures.

Acknowledgements

We wish to thank, especially, J Kaźmierczak and B Kremer for organizing the sampling expedition to Lake Alchichica in 2007 and for providing invaluable help during sampling to PLG and DM This project was financed by the French Interdisciplinary program 'Environnements planétaires et origines de la vie' (PID OPV-EPOV 2010). We thank the Region Ile de France for the participation in the financing of the IPGP Confocal/Raman microscope (Sesame project 2005).

References

Amann R, Fuchs BM. (2008). Single-cell identification in microbial communities by improved fluorescence in situ hybridization techniques. *Nat Rev* **6**: 339–348.

Arp G, Reimer A, Reitner J. (2003). Microbialite formation in seawater of increased alkalinity, Satonda Crater Lake, Indonesia. *J Sediment Res* **73**: 105–127.

Arp G, Reimer A, Reitner J. (1999). Calcification in cyanobacterial biofilms of alkaline salt lakes. *Eur J Phycol* **34**: 393–403.

Arp G, Reimer A, Reitner J. (2001). Photosynthesis-induced biofilm calcification and calcium concentrations in Phanerozoic oceans. *Science* **292**: 1701–1704.

Awramik SM, Sprinkle J. (1999). Proterozoic stromatolites: the first marine evolutionary biota. *Hist Biol* **13**: 241–253.

Benzerara K, Menguy N, Lopez-Garcia P, Yoon TH, Kaźmierczak J, Tyliszczak T *et al*. (2006). Nanoscale detection of organic signatures in carbonate microbialites. *Proc Natl Acad Sci USA* **103**: 9440–9445.

Benzerara K, Menguy N. (2009). Looking for traces of life in minerals. *Compt Rend Palevol* **8**: 617–628.

Beyssac O, Lazzeri M. (2012). Application of Raman microspectroscopy to the study of graphitic carbon materials in Earth Sciences. In: Dubessy J, Caumon M-C, Ruff F (eds). *EMU Notes in Mineralogy-Applications of Raman spectroscopy to Earth sciences and cultural heritage*. Mineralogical Society: Twickenham, UK, Chapter 12.

Braissant O, Cailleu G, Dupraz C, Verrecchia EP. (2003). Bacterially induced mineralization of calcium carbonate in terrestrial environments: the role of exopolysaccharides and amino acids. *J Sediment Res* **73**: 485–490.

Braissant O, Decho AW, Dupraz C, Glunk C, Przekop KM, Visscher PT. (2007). Exopolymeric substances of sulfate-reducing bacteria: interactions with calcium at alkaline pH and implication for formation of carbonate minerals. *Geobiology* **5**: 401–411.

Braissant O, Decho AW, Przekop KM, Gallagher KL, Glunk C, Dupraz C *et al.* (2009). Characteristics and turnover of exopolymeric substances in a hypersaline microbial mat. *FEMS Microbiol Ecol* **67**: 293–307.

Buick R, Dunlop JSR, Groves DI. (1981). Stromatolite recognition in ancient rocks: an appraisal of irregularly laminated structures in an Early Archaean chert-barite unit from North Pole, Western Australia. *Alcheringa* **5**: 161–181.

Büdel B, Rhiel E. (1985). A new cell wall structure in a symbiotic and free-living strain of the blue-green alga genus *Chroococcidiopsis* (Pleurocapsales). *Arch Microbiol* **143**: 117–121.

Couradeau E, Benzerara K, Gérard E, Estève I, Moreira D, Tavera R *et al.* (2013). Cyanobacterial calcification in modern microbialites at the submicrometer-scale. *Biogeosci Discuss* **10**: 3311–3339.

Couradeau E, Benzerara K, Gérard E, Moreira D, Bernard S, Brown Jr GE *et al.* (2012). An early-branching microbialite cyanobacterium forms intracellular carbonates. *Science* **336**: 459–462.

Couradeau E, Benzerara K, Moreira D, Gérard E, Kazmierczak J, Tavera R *et al.* (2011). Prokaryotic and eukaryotic community structure in field and cultivated microbialites from the alkaline lake of Alchichica (Mexico). *PloS ONE* **6**: e28767.

Decho AW, Visscher PT, Reid RP. (2005). Production and cycling of natural microbialexopolymers (EPS) within a marine stromatolite. Palaeogeography, Palaeoclimatology. *Palaeoecology* **219**: 71–86.

Deleuze M, Brantley SL. (1997). Inhibition of calcite crystal growth by Mg^{2+} at 100°C and 100 bars: influence of growth regime. *Geochim Cosmochim Acta* **61**: 1475–1485.

Dill RF, Shinn EA, Jones AT, Kelly K, Steinen RP. (1986). Giant subtidal stromatolites forming in normal salinity waters. *Nature* **324**: 55–58.

Downs RT. (2006). The RRUFF Project: an integrated study of the chemistry, crystallography, Raman and infrared spectroscopy of minerals. *Program and Abstracts of the 19th General Meeting of the International Mineralogical Association in Kobe, Japan* O03-13.

Dravis JJ. (1983). Hardened subtidal stromatolites, Bahamas. *Science* **219**: 385–386.

Dupraz C, Reid RP, Braissant O, Decho AW, Norman RS, Visscher PT. (2009). Processes of carbonate precipitation in modern microbial mats. *Earth Sci Rev* **96**: 141–152.

Dupraz C, Visscher PT. (2005). Microbial lithification in marine stromatolites and hypersaline mats. *Trends Microbiol* **13**: 429–438.

Foster JS, Green SJ, Ahrendt SR, Golubic S, Reid RP, Hetherington KL *et al.* (2009). molecular and morphological characterisation of cyanobacterial diversity in the stromatolites of highborne Cay, Bahamas. *ISME J* **3**: 573–587.

Goh F, Allen MA, Leuko S, Kawaguchi T, Decho AW, Burns BP *et al.* (2009). Determining the specific microbial populations and their spatial distribution within the stromatolite ecosystem of Shark Bay. *ISME J* **3**: 383–396.

Grotzinger JP, Knoll AH. (1999). Stromatolites in Precambrian carbonates: evolutionary mileposts or environmental dipsticks? *Annu Rev Earth Planet Sci* **27**: 313–358.

Hall EK, Singer GA, Polzl M, Hammerle I, Schwarz C, Daims H *et al.* (2010). Looking inside the box: using Raman microspectroscopy to deconstruct microbial biomass stoichiometry one cell at a time. *ISME J* **5**: 196–208.

Huang WE, Fergusson A, Singer AC, Lawson K, Thompson IP, Kalin RM *et al.* (2009). Resolving genetic functions within microbial population: *in situ* analyses using rRNA and mRNA stable isotope probing coupled with single-cell-Raman-fluorescence *in situ* hybridization. *Appl Environ Microbiol* **75**: 234–241.

Huang WE, Mengqiu L, Jarvis RM, Goodacre R, Banwart SA. (2010). Shining light on the microbial world: the application of Raman microspectroscopy. *Adv Appl Microbiol* **70**: 153–186.

Huang WE, Stoecker K, Griffiths R, Newbold L, Daims H, Whiteley AS *et al.* (2007). Raman-FISH: combining stable isotope Raman spectroscopy and fluorescence in situ hybridization for single cell analysis of identity and function. *Environ Microbiol* **9**: 1878–1889.

Kah LC, Knoll AH. (1996). Microbenthic distribution of Proterozoic tidal flats: environmental and taphonomic considerations. *Geology* **24**: 79–82.

Kawaguchi T, Decho AW. (2002). In situ microspatial imaging using two-photon and confocal laser scanning microscopy of bacteria and extracellular polymeric secretions (EPS) within marine stromatolites. *Marine Biotechnol* **4**: 127–131.

Kaźmierczak J, Kempe S, Kremer B, López-García P, Moreira D, Tavera R. (2011). Hydrochemistry and microbialites of the alkaline crater lake Alchichica, Mexico. *Facies* **57**: 543–570.

Kempe S, Kaźmierczak J, Landmann G, Konuk T, Reimer A, Lipp A. (1991). Largest known microbialites discovered in Lake Van, Turkey. *Nature* **349**: 605–608.

Kempe S, Kaźmierczak J. (1993). Satonda Crater Lake, Indonesia: Hydrogeochemistry and biocarbonates. *Facies* **28**: 1–31.

Kempe S, Kaźmierczak J. (1994). The role of alkalinity in the evolution of ocean chemistry, organization of living systems, and biocalcification processes In: Doumenge F, Allemand D, Toulemont A (eds). *Past and Present Biomineralization Processes. Considerations About the Carbonate Cycle*. Institut Océanographique: Monaco, pp 61–117.

Knoll AH, Semikhatov MA. (1998). The genesis and time distribution of two distinctive proterozoic stromatolite microstructures. *Palaios* **13**: 408–422.

Komárek J, Hauer T. (2011). *CyanoDB.cz On-line database of cyanobacterial genera*. Univ. of South Bohemia and Inst. of Botany AS CRhttp://www.cyanodb.cz.

Kremer B, Kaźmierczak J, Stal LJ. (2008). Calcium carnonate precipitation in cyanobacterial mats from sandy tidal falts of the North Sea. *Geobiology* **6**: 46–56.

Lepot K, Benzerara K, Brown GEJ, Philippot P. (2008). Microbially influenced formation of 2.724-million-year-old stromatolites. *Nat Geosci* **1**: 118–121.

Lepot K, Benzerara K, Brown GEJ, Philippot P. (2009). Organic matter heterogeneity in 2.72 Ga stromatolites: alteration versus preservation by sulphur incorporation. *Geochim Cosmochim Acta* **73**: 6579–6599.

Logan BW. (1961). *Cryptozoon* and associated stromatolites from the recent, Shark Bay, Western Australia. *J Geol* **69**: 517–533.

López-García P, Kaźmierczak J, Benzerara K, Kempe S, Guyot F, Moreira D. (2005). Bacterial diversity and carbonate precipitation in the giant microbialites from the highly alkaline Lake Van, Turkey. *Extremophiles* **9**: 263–274.

Ludwig R, Al-Horani FA, de Beer D, Jonkers HM. (2005). Photosynthesis-controlled calcifification in a hypersaline microbial mat. *Limnol Oceonogr* **50**: 1836–1843.

Moran AL. (2000). Calcein as a marker in experimental studies newly-hatched gastropods. *Marine Biol* **137**: 893–898.

Obst M, Dynes JJ, Lawrence JR, Swerhone GDW, Benzerara K, Karunakaran C *et al.* (2009). Precipitation of amorphous CaCO3 (aragonite-like) by cyanobacteria: ASTXM study of the influence of EPS on the nucleation process. *Geochim Cosmochim Acta* **73**: 4180–4198.

Planavsky N, Reid RP, Lyons TW, Myshrall KL, Visscher PT. (2009). Formation and diagenesis of modern marine calcified cyanobacteria. *Geobiology* **7**: 566–576.

Reid RP, Browne KM. (1991). Intertidal stromatolites in a fringing Holocene reef complex in the Bahamas. *Geology* **19**: 15–18.

Reid RP, James NP, Macintyre IG, Dupraz CP, Burne RV. (2003). Shark Bay stromatolites: microfabrics and reinterpretation of origins. *Facies* **49**: 45–53.

Reid RP, Visscher PT, Decho AW, Stolz JF, Bebout BM, Dupraz C *et al.* (2000). The role of microbes in accretion, lamination and early lithification of modern marine stromatolites. *Nature* **406**: 989–992.

Rividi N, Van Zuilen M, Philippot P, Menez B, Godard G, Poidatz E. (2010). Calibration of carbonate composition using micro-Raman analysis: application to planetary surface exploration. *Astrobiology* **10**: 293–309.

Schultze-Lam S, Beveridge TJ. (1994). Nucleation of celestite and strontianite on a cyanobacterial S-layer. *Appl Environ Microbiol* **60**: 447–453.

Stanley SM, Hardie LA. (1999). Hypercalcification: paleontology links plate plate tectonics and geochemistry to sedimentology. *GSA Today* **9**: 1–7.

Wagner M, Ivleva NP, Haisch C, Niessner R, Horn H. (2009). Combined used of confocal laser scanning microscopy (CLSM) and Raman Microscopy (RM): investigation on EPS-matrix. *Water Res* **43**: 63–76.

Wagner M. (2009). Single-cell ecophysiology of microbes as revealed by Raman microspectroscopy or secondary ion mass spectrometry imaging. *Annu Rev Microbiol* **63**: 411–429.

Waterbury JB, Stanier RY. (1978). Patterns of growth and development in Pleurocapsalean cyanobacteria. *Microbiol Rev* **42**: 2–44.

Zeebe RE, Wolf-Gladrow DA. (2001). In *CO_2 in Seawater: Equilibrium, Kinetics, Isotopes.* Halpern D (ed. 65. Elsevier Oceanography Series: Amsterdam, pp 346.

Zippel B, Neu TR. (2011). Characterization of glycoconjugates of extracellular polymeric substances in tufa-associated biofilms by using fluorescence lectin-binding analysis. *Appl Environ Microbiol* **77**: 505–516.

Supplementary Information accompanies this paper on The ISME Journal website (http://www.nature.com/ismej)